Al Azhar Bulletin of Science Vol. 29, No. 2 (December), 2018, pp. 125-142.

INTEGRATION OF GEOSPATIAL TECHNIQUES FOR MAPPING GROUNDWATER POTENTIALITIES IN EL-QAA PLAIN, SOUTHWEST SINAI, EGYPT

M. Y. Zein El-Din[1], Mostafa AbuBakr[1], Ramadan G. Hroun[2], Mamdouh M. Ali[2]

[1] *Geology Department, Al-Azhar University, Nasr City, Cairo, Egypt*
[2] *The Egyptian Mineral Resources Authority (EMRA), Cairo, Egypt*

ABSTRACT

Groundwater represents the essential source of fresh water in most arid regions, such as the Sinai Peninsula. Exploration of groundwater resources in dry lands requires survey of vast areas with conventional land-based techniques. This study performs criteria for groundwater probabilities in the southwestern part of Sinai Peninsula by mapping Groundwater Potential (GWP) using advanced remote sensing and geospatial techniques along with field validation, as a complemented tool for the conventional land-based methods. The main goal of this work is delineating groundwater recharging by identifying and examining the influence of physiographic variables that affecting groundwater storage. Therefore, multi-sensors remote sensing data from ASTER, Landsat-8, MODIS, Shuttle Radar Topography Mission (SRTM), Tropical Rainfall Measuring Mission (TRMM), and Radarsat-1 were used to construct several geospatial thematic layers (variables). These layers include elevation, slope, curvature, drainage density, topographic wetness index, surface roughness, frequency of thermal anomaly, accumulated precipitation, Land Use/Land Cover (LULC) and lineament density. All variables were arranged and weighted based on their contributions in groundwater recharge through infiltration and percolation processes of near surface aquifers. The Simple Additive Weight (SAW) method was adopted for computing the variables weights and producing the GWP map. This aggregated map was then classified into 5 classes, from very high to very low potentiality zones. The highest GWP zone was defined along Wadi El-Awaj, the northern part of Wadi Araba, and near the outlets of several wadies south of El-Tour City. The GWP was observed to be associated with low terrain, high surface ruggedness, increased drainage and lineament densities, and relatively close to thermal anomalies in wadi deposits and adjacent sandy areas. The results were validated by field observations including, soil infiltration rate, water wells data and vegetation patterns in the study area. Based on the outcomes, remote sensing data along with geospatial techniques can provide a powerful tool for groundwater probabilities in arid lands, and thus can be applied in regions with similar conditions, such as the Middle East countries.

Key words*:* GWP, Remote sensing, Geospatial techniques, El-Qaa, Groundwater in Sinai

1. INTRODUCTION

Recently fresh water resources on Earth, especially in arid lands, are severely stressed by the rapid growth of population and development projects. The world bank considered the Middle East the most water scarce region in the world, where water availability is below the global average of 7000 m^3 /person/year at an estimated 1200 m^3 /person/year (The World Bank, 2010). This situation is more significant in Egypt due to the increasing population (104 million, about 2.56 m/y) and limited water supplies (55.5 billion m^3/y). Consequently, the United Nation warning that Egypt could face serious water shortage on 2020. Therefore, the Egyptian government is paying huge attention to find alternative renewable water resources, which would be the base for establishing new communities outside the overpopulated Nile Delta and the Nile Valley.

Sinai Peninsula is represented one of these dire situations; therefore, it has high priority in the government development planning due to its strategic and national importance. This special attention is essentially attributed to its unique location between the largest continents on the Earth. It has been served as a bridge connecting northeast Africa with West Asia. Although Sinai Peninsula suffers a scarcity of fresh water, because it is among the most arid desert in the world (40 mm/y.); however, the geologic criteria indicates that it could contain high groundwater potentiality (Sultan et al.,

2011). This assumption was based on the wet climate periods, which alternated between arid and wet throughout the Quaternary Period, with the last of the major wet periods occurring in the Holocene (9500–4500 y. BP).

El - Qaa plain area covers an area of about 4100 km^2 and it is not clearly flat area, but it is dissected by many wadies, terraces, playas and alluvial fans, which produced during long fluvial periods that occurred during the Pleistocene time over the plain (Ahmed, 1984). Part of this water was infiltrated and stored in the shallow aquifers. Nowadays, recharging process are still taking place through sporadic rainstorms, which flow through a dense drainage network to the Gulf of Suez at El-Tour City. Mapping these groundwater potentialities with conventional techniques, such as geophysical tools, is very difficult and time-consuming task in such vast areas. Therefore, the present work aims at delineating groundwater accumulation by identifying and examining the influence of physiographic features of sub-basins that affecting groundwater recharge and storage. For this end, multi-sensor remote sensing data and geospatial technique along with field validation were utilized for mapping Groundwater Potential (GWP) in El-Qaa Plain, as a supplemented tool for the conventional geophysical methods. This relatively new technique was applied successfully in regions with similar climatic conditions (Amer et al., 2013; Elbeih, 2014; Abrams et al., 2018).

Although many authors have investigated the groundwater potentialities in the study area, (e.g., Ahmed, 1984; Helba, 1987; Masoud, 2009) none of these studies have used exclusively remotely derived data to model potential sites for groundwater accumulation in the entire El-Qaa plain. Ahmed (1984) studied the geomorphology and the hydrogeology of El-Qaa plain based on field investigations with the aid of little amount of aerial photographs. Helba (1987) investigated, for the first time, the geology of Gebel Safariat area which lies in the northern part of the plain. Masoud (2009) used runoff modeling to estimate flash flood and groundwater recharge potential for the whole area of South Sinai. Ahmed (2012) applied both gravity and magnetic data over the area of El-Qaa plain by using 381 ground gravity stations and 800 lines of aeromagnetic data to investigate the hydrogeologic and structural settings, areal distribution, geometry, and water storage of deep aquifers in El Qaa plain.

Most of the previous studies used conventional tools to estimate either the groundwater recharge potentialities or flash flood risks at some parts of the investigated plain. Therefore, the current study will employ the powerful coverage of the remote sensing data and geospatial technique to indirectly detect zones with high groundwater probabilities within the entire area of El-Qaa Plain.

2. STUDY AREA

The study area locates in Sinai Peninsula, which is an extension of the Great Sahara, the driest deserts on terrestrial. This triangular block of land occupies 61,000 km^2, bounded to the North and the South by the Mediterranean and Red Seas, respectively, while the Suez Canal and the Gulf of Suez are bordered it from the west, and the Arabian Rift Valley (Gulf of Aqaba) with the Negev Desert from the east. El-Qaa plain is located in the southwestern part of the peninsula.

El-Qaa Plain is situated between latitudes 27° 47` & 28° 43` N and longitudes 33° 21` & 34° 13` E. The plain itself is a structural depression trending NNW-SSE, parallel to the main rift system of the Gulf of Suez (Azab & El-Khadragy, 2013). The depression running for approximately 150 km and 20-30 km wide.

The plain is covered by a thick Quaternary deposits (mainly sand and gravels with clay and silt) of more than 1 km overlying basement and Phanerozoic deposits (JICA, 1999). The eastern mountains is composed mainly of igneous and metamorphic rocks of red and grey granites together with gneisses (Dames and Moore, 1981). Another small array of igneous rocks of

the same type of the eastern mountains occurring to the south of the plain towards Ras Mohammed. Sedimentary rocks consist mainly of carbonates and sandstones crops out in the northern side of the plain forming Gebel Qabliat and Gebel Safariat, while the rest of the plain is covered by recent deposits (Fig. 1).

The plain slopes from the north to the south and from east to west (Dames and Moore, 1981), and it is dissected by 45 wadies flow from the eastern mountains and their channels were buried in the plain through different cycles of sedimentation during Quaternary time (Khalil & Hendy, 1984). Some wadies, like Wadi Abyad, Wadi Waraka, Wadi Meir and Wadi Wigran, are draining directly into Wadi El-Awaj, which is the longest wadi in the study area with outlet at El-Tour City. There are some isolated hills of basement rocks with an elevation of about 400 to 500m a.s.l. as Gebel Karien Attot south of the plain (Gemail, 1996). Most of the plain is generally characterized by gentle slope of lower than 200 m a.s.l. (Fig. 1).

The climatic conditions of the plain are similar to the whole Peninsula which falls within the great arid climatic belt crossing northern Africa and southwestern Asia. In the summer the mean daily maximum temperatures is 28°C to 37°C in the North, 31°C to 42°C near the south coast, while the minimum temperatures may fall around 6°C to 10°C in the winter.

There are six meteorological stations in Southern Sinai including Sharm El-Sheikh, El-Tour, Abu Rudeis, Ras Sudr, St. Catherine and Nekhel. Regular records are absent for the majority of these stations as they were stopped after the 1967 war and renewed after 1982 (Sherief, 2008). According to (Salem, 1990) the mean annual rainfall ranges between 10.4 mm / year at El-Tour, 15.4 mm / year at Ras Sudr, 21.5 mm / year at Abu Rudeis, and 63 mm / year at St. Catherine.

3. DATA AND METHODOLOGY

Compared to conventional methods that seek water through geophysical investigations and drilling wells into aquifers, the combination of remote sensing and GIS techniques with field validation can provide a

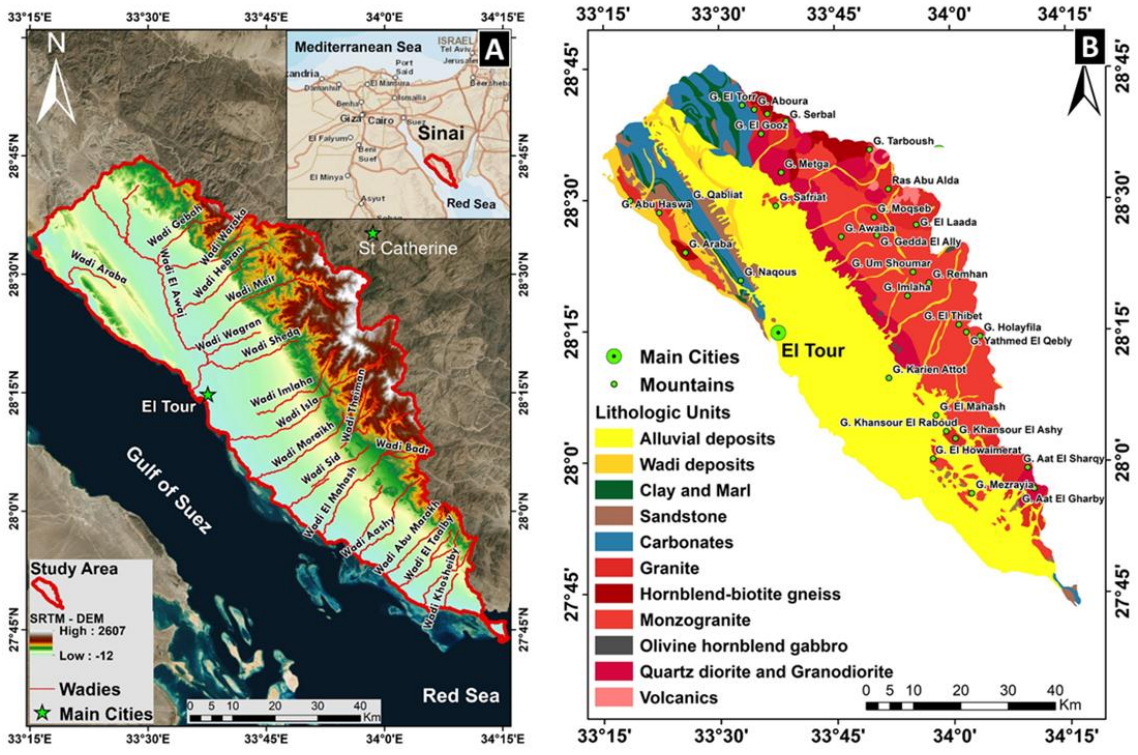

Fig. 1: (A) Location map overlaid with topographical Digital Elevation Model (DEM) for the study area, (B) Geologic map of El-Qaa Plain (modified after EGSMA, 1994).

promising tool for detecting and harnessing sustainable water resources. Therefore, the present work relied basically on optical, radar and thermal remote sensing data for mapping groundwater potentiality, especially in the light of lack of surface flow data in the study area. The data types were selected to represent the physiographic influence (variables) on groundwater accumulation. The adopted methodology utilized the weighted index overlay analysis technique for computing the variables weights and producing the GWP map. These variables were extracted from remotely sensed data to make the proper integration between them in order to predict the shallow groundwater potentiality sites. The workflow for the utilized data and methods consists of two main procedures; first, variable extraction using the compiled remote sensing data products and second, the GWP analysis and modelling (Fig. 2).

3.1. Remote Sensing Data

Orbital remote sensing technology has progressed to advanced levels of practical application, particularly with respect to optical, radar and thermal-infrared imagery. Optical imagery can be utilized to map surface features, present land cover/use, vegetation distribution patterns in addition to lithological details of the study area. Space-borne radar images, on the other hand, are a powerful tool in mapping surface roughness and sand-buried fluvial features such as paleo river courses and lakebeds (e.g., Mccauley et al., 1982; Ghoneim & El-Baz, 2007; AbuBakr et al., 2013). In addition, the Shuttle Radar Topography Mission (SRTM) is the most common source of Digital Elevation Model (DEM) and powerful in delineating the surface drainage networks (e.g., Ghoneim et al., 2007). Thermal-infrared (TIR) can be used to trace near-surface moisture content accumulations following rainfall events particularly in sandy deserts (e.g., Ghoneim, 2008), such as the area under investigation.

In this study, optical, radar and thermal data were utilized, including the Advanced Spaceborne Thermal Emission and Reflection (ASTER), Operational Land Imager (OLI), Moderate Resolution Imaging Spectroradiometer (MODIS), Shuttle Radar Topography Mission (SRTM), Tropical Rainfall Measuring Mission (TRMM), and Radarsat-1. These wide set of data were downloaded from the USGS and NASA's websites, which are open sources except the Radarsat-1 image was provided by the Center for Remote Sensing at Boston University (Table 1).

3.2. Methodology

According to the workflow in fig. 2, the adopted methodology was divided into two main parts 1- the construction of the required thematic layers and 2- the groundwater potentiality modelling.

3.2.1. Construction of the Required Thematic Layers

Ten thematic layers (variables) were extracted from satellite data including elevation, slope, curvature, drainage density, Topographic Wetness Index (TWI), surface roughness, frequency of thermal anomaly, accumulated precipitation, Land Use/Land Cover (LULC) and lineament density. These variables will be mentioned in detail in the following sections based on their data sources.

3.2.1.1. Elevation and DEM derived layers

The Digital Elevation Model (DEM) data were constructed by mosaicking 4 tiles of SRTM 1Arc-Second, and then subset the mosaic to match the boundary of El-Qaa Plain. The spatial analyst tools in ArcGIS 10.4 was used to produce the slope, standard curvature and drainage density layers (Fig. 3A, B, C and D). The slope and curvature provide an understanding to the infiltration conditions in the study area. The slope measures the change of relief per degrees (raster unit) and thus provide insight of runoff acceleration from uphill to downhill. The slope (degrees) layer was generated directly from the DEM using the surface tools in ArcGIS. The SRTM-DEM was also utilized to extract the standard curvature layer, which gives an indicator of the concavity and convexity of the ground surface as positive

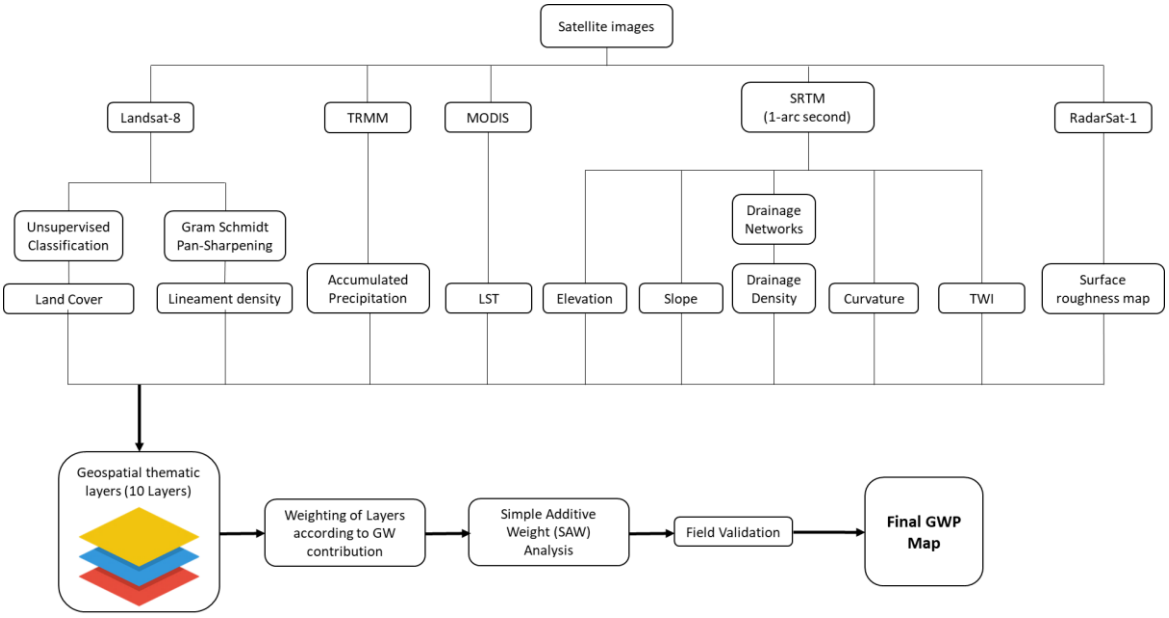

Fig 2: Simplified workflow for the remote sensing data and the methodology, 1) construction of thematic layers, 2) groundwater potentiality modeling.

Table 1: Remote sensing data description, sources and associated layers.

Sensor	Source	Data	Spatial Resolution	Generated Thematic Layer
Shuttle Radar Topography Mission (SRTM)	USGS Earth Explorer [https://earthexplorer.usgs.gov/]	Digital Elevation Model (DEM)	30m	Elevation, Slope, Curvature, Drainage Density, Topographic Wetness Index
Advanced Spaceborne Thermal Emmision ReVection Radiometer (ASTER)	USGS Earth Explorer [https://earthexplorer.usgs.gov/]	Level 1T Multispectral Imagery	15m VNIR, 30m MIR, 90m TIR	Landcover
Tropical Rainfal Measuring Mission (TRMM)	Nasa Giovanni https://giovanni.gsfc.nasa.gov/giovanni/	Radar Precipitation Measurements	1/4th Degree (27km)	Accumulated Precipitation
Moderate Resolution Imaging Spectroradiometer (MODIS)	USGS Earth Explorer [https://earthexplorer.usgs.gov/]	Daily Daytime Land Surface Temperature	1km	Land Surface Temperature
Landsat-8 Operational Land Imager	USGS Earth Explorer [https://earthexplorer.usgs.gov/]	Multispectral Imagery	30m	Landcover, Lineament Density
Radarsat-1	The Center for Remote Sensing in Boston University	C-band Radar, HH Polarization	12.5m	Surface Roughness

and negative values, respectively. In addition, the surface flow direction was computed using the eight directions model (D3) according to Jenson and Dominque (1988). Flow accumulation was then deduced and the drainage network was defined using 1000 threshold. Finally, a drainage density map was extracted, based on the drainage patterns, which were calculated in square kilometer.

3.2.1.2. Topographic Wetness Index (TWI):

This index was developed by Beven and Kirkby (1979) and it is considered the steady state wetness index, which commonly used to quantify the topographic control on hydrological processes (Sørensen et al., 2006). The TWI is commonly used (e.g., Abrams et al., 2018) to estimate the influence of topography and soil moisture based on the previously generated slope and flow accumulation layers. The TWI layer was calculated using the following equation:

$$\ln\left(\frac{a}{\tan b}\right)$$

where, a is the upslope area of a given cell and b is the slope in radians.

The TWI was generated using the aforementioned equation in the raster calculator in ArcGIS software (Fig. 4A).

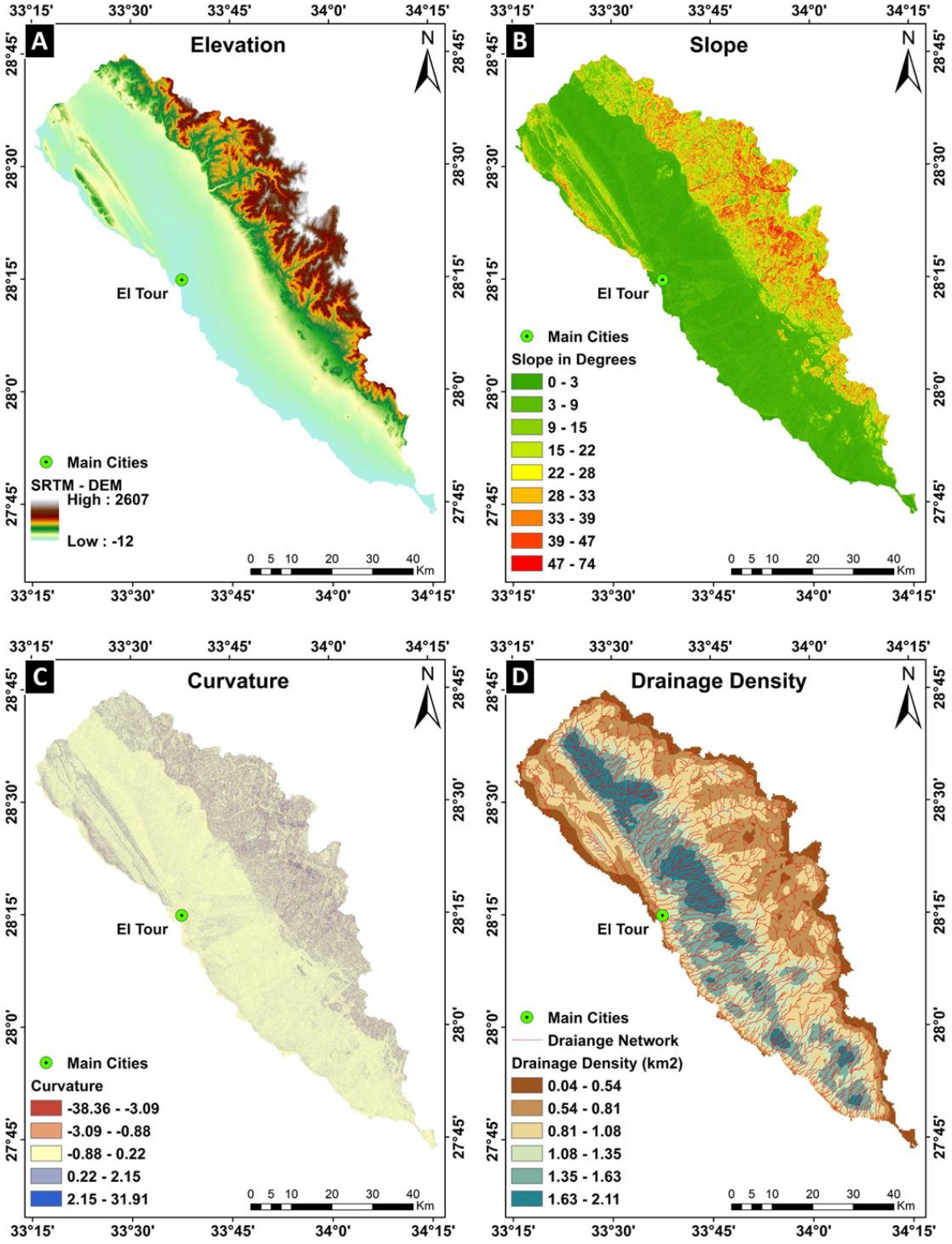

Fig. 3: Elevation and DEM derived layers: (A) Elevation, (B) Slope, (C) Curvature, (D) Drainage Density.

3.2.1.3. Surface Roughness

Surface roughness (SR) has strong impact on the microwave signals, it can be detected using radar backscattering waves (Gaber et al., 2011). The microwave with shorter wavelength of C-band could be more sensitive to slight changes in wadi surface roughness (micro-roughness) than the L-band with its longer wavelength, which has more penetration depth (Lee and Pottier, 2017). Therefore, Radarsat-1 satellite images was used to create the surface roughness map of the study area, which can differentiate between the diversity of texture for the surface deposits in form of five classes: very rough, rough, medium, fine and very fine materials (Fig. 4B).

3.2.1.4. Land Surface Temperature (LST)

Although rainfall events in Sinai are occasional, monitoring thermal variation in bare sandy surface following a rainfall event could provide indirect indications to groundwater accumulations (AbuBakr, 2014). This layer aims at locating and investigating thermal anomalies in El-Qaa Plain to locate near surface groundwater accumulation, using thermal remote sensing data. It is here attempted to reveal possible connection between these anomalies and the groundwater infiltration. This method was used successfully to detect groundwater in similar arid lands, such as North Sinai Peninsula and the United Arab Emirates (AbuBakr, 2014; Ghoneim, 2008).

A Systematic analysis for thermal infrared (TIR) data of daily MODIS LST were extracted from MODIS MYD11A1 V6 image, which provides per-pixel land surface temperature (LST) in a 1200 x 1200 kilometer grid (Wan et al., 2015). MODIS tiles were re-projected from its original Sinusoidal (ISIN) projection to UTM-36N projection and combined together, then clipped to the study area boundary and finally the pixel values converted from Kelvin to Celsius degrees (Fig. 4C).

3.2.1.5. Accumulated Precipitation

Due to the lack of rainfall monitoring stations in the study area, the Tropical Rainfall Measuring Mission (TRMM) was used to estimate the accumulated precipitation. TRMM is a joint space mission between NASA and the Japan Aerospace Exploration Agency (JAXA) designed to monitor and study tropical rainfall. This mission provides global rainfall data with a 0.25° × 0.25° footprint since 1997. Despite the coarse resolution of the satellite rainfall products, they are used in a wide range of applications due to there are being cost effective and available for the globe (Harris et al., 2007). Thus, TRMM was employed here to estimate the amount of rainfall event that was occurred between 2012 to 2018.

The precipitation data was extracted using TRMM 3B43 V7 for 6 years (from 2012 to 2018), which was downloaded from *https://giovanni.gsfc.nasa.gov/giovanni/* website. The TRMM data were converted from netcdf format to vector points then an interpolation process was applied using spline method to convert back the point vectors to interpolated raster, which was then clipped and adjusted to the extent of the investigated area (Fig. 4D).

3.2.1.6. Land Use/Land Cover (LULC)

The LULC is significant for mapping the variation in soil types and anthropogenic activities in the plain area, which is critical for runoff infiltration. These layers were produced from the OLI sensor, which mounted on the Landsat-8. Several pre-processing analyses were applied including the atmospheric correction, which removes the effects of the atmosphere (scattering and absorption) and the DN was ultimately converted to surface radiance. After that, a Principal Component Analysis (PCA) was carried out as an image transformation technique to enhance the spectral resolution of the images to reduce the redundancy of the data before going through the image classification (Lillesand & Kiefer, 1987). Another step was performed prior image classification, which is the extraction and masking the vegetation in the study area through applying the Normalized Difference Vegetation Index (NDVI) (Weier & Herring,

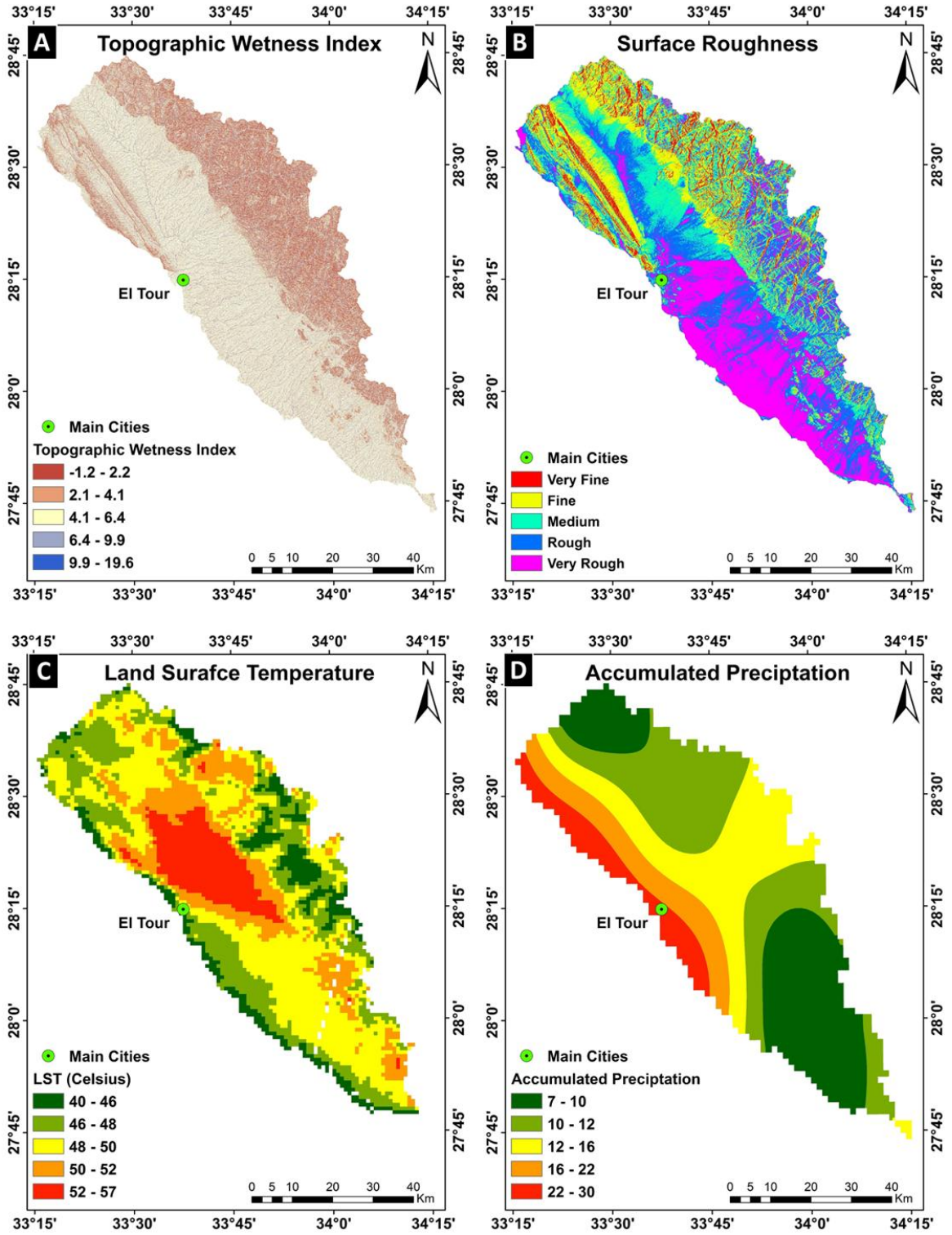

Fig. 4: (A) Topographic wetness Index, (B) Surface Roughness, (C) Land Surface Temperature, (D) Accumulated Precipitation.

2018). The resulted vegetation vector layer compared with the OLI image using a false band combination (bands 5,4,3 in RGB, respectively) as a verification step before proceeding to the classification process.

A K-Means classification method was adopted to classify the landcover in study area. The technical classification parameters comprised of a threshold of 5%, maximum iterations of 50 to produce 20 classes. The spectrally similar classes were merged together according to the surface lithology and the type of land use with the aid of the published geological map (EGSMA, 1994) and high resolution imagery in Google Earth. The final product involved 5 classes of LULC: basement rocks, old alluvial deposits, recent and wadi deposits, sedimentary rocks, urban & roads and vegetation (fig. 5A).

3.2.1.7. Lineament Density

The accuracy of the lineament extraction from optical satellite images relied on the sensor characteristics, spatial and spectral resolution, and weather-illumination conditions (Smith & Wise, 2007) Therefore, lineaments were extracted from the Landsat-8 images after applying the Gram-Schmidt transformation to enhance the spatial resolution of the multispectral OLI image (Laben & Brower, 2000). The lineaments then extracted and exported to Google Earth software in order to verify them for eliminating the false lineaments like roads, tracks, and other human (artificial) activities. Ultimately, the surface lineaments were extracted and a line density layer was produced, using the same processing routine of the drainage density layer, (Fig. 5B).

3.2.2. Groundwater Potentiality Indexing and Modelling

It is pointless to perform the groundwater potentiality modeling directly on the extracted thematic layers without a weighted index connecting them together based on their groundwater contribution. Therefore, a semi-quantitative weighted index (GWP indexing) was used to divide each thematic layer into only 5 classes.

3.2.2.1. Semi-Quantitative Weighted Index

This indexing has been developed based on the authors previous experience in geologic,

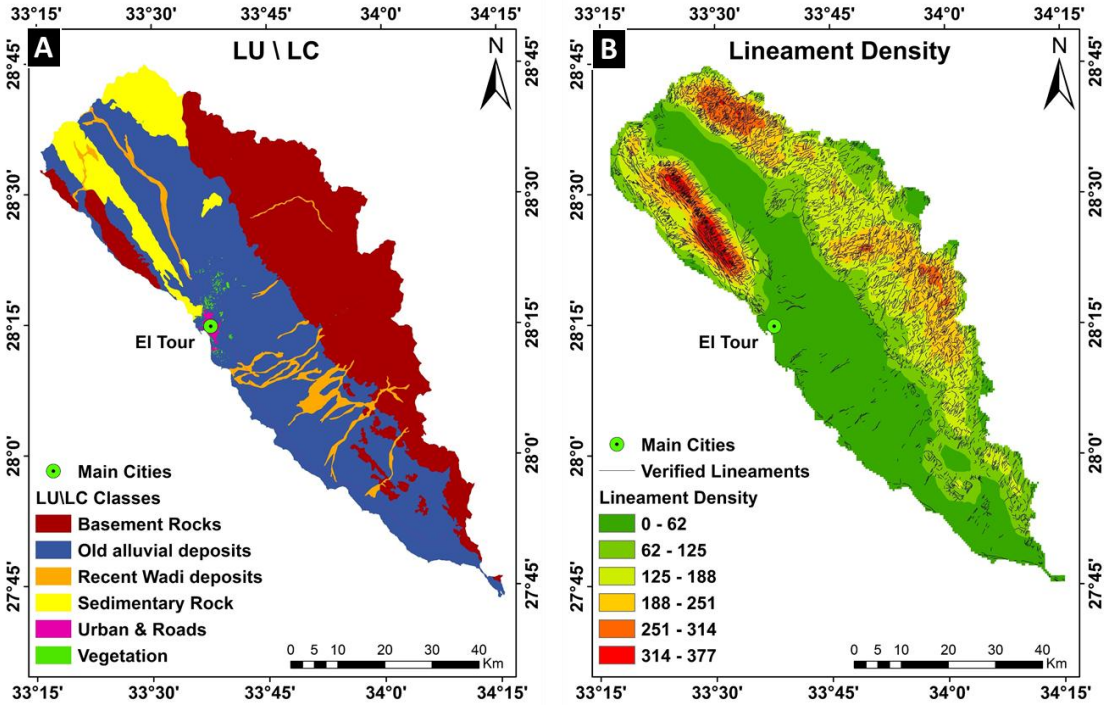

Fig. 5: (A) Land Use/Land Cover (LU\LC), (B) Lineament Density.

hydrogeologic, and geospatial researches in some regions with similar conditions (e.g., AbuBakr et al., 2013; Abrams et al., 2018). Furthermore, field investigations in the study area and literature review were significantly contributed in the assignment of the GWP indexing.

The layers with continuous values were divided into five classes using natural break (Jenks) method (Jenks, 1967), to represent the range and distribution of values across the study area (Table 2). Each class was assigned to a common scale value, which could range from 0 to 100 as an estimate of contribution in the GWP for generating the final form of the thematic layers (fig. 6, 7 and 8). Larger scale value indicative to higher GWP and vice versa. For instance, the very high elevation and steep slope represent very low contribution (0-20) in GWP, while very low elevation and gentle slope reflect very high to high contribution (80-100) in GWP (Table 2).

3.2.2.2. Simple Additive Weight method (SAW)

There are several techniques of GWP overlay modelling, most of them have been tested and estimated, such as Probabilistic Frequency Ratios (PFR) (Manap et al., 2013; Naghibi et al., 2015), the Analytical Hierarchy Process (AHP) (Adiat et al., 2012; Mallick et al., 2015), and the Simple Additive Weight (SAW) (Abrams et al., 2018; Al-Ruzouq, Shanableh, & Merabtene, 2015). According to these studies, especially Abrams et al., 2018 the Simple Additive Weight method (SAW) is probably one of the most effective methods for modeling groundwater potential.

The SAW technique is the most primitive of the semi quantitative index-overlay techniques. It assigns equal weight to all variables (layers) and assuming that the assigned GWP values are adequate to represent potentiality (Abrams et al., 2018). Therefore the 10 weighted thematic layers were summed together using the following SAW formula:

$$GWP_{SAW} = \sum GWP_E, GWP_S, GWP_{DD}, GWP_{LD}, GWP_C, GWP_{LC}, GWP_{SR}, GWP_{LST}, GWP_{TWI}, GWP_{AP}$$

where, GWP_S, is the SAW technique for all groundwater potential, GWP_E potential for elevation, GWP_S potential for slope, GWP_{DD} potential for drainage density, GWP_{LD} potential for lineament density, GWP_C potential for curvature, GWP_{LC} potential for landcover, GWP_{SR} potential for surface roughness, GWP_{LST} potential for land surface temperature, GWP_{TWI} potential for topographic wetness index and GWP_{AP} is the potential for accumulated precipitation.

Table 2: All variables and weights according to contribution to GW

variables \ weight	20	40	60	80	100
1- Elevation (m)	v. high	high	medium	low	v. low
	1500 – 2600	1500 – 1000	1000 - 600	600 - 250	250 - 0
2- Slope (degree)	v. high	high	medium	low	v. low
	37 - 74	27 - 37	17 - 27	7 - 17	0 -7
3- Curvature	v. low	low	medium	high	v. high
	(-38) – (-3)	(-3) – (0)	0 – 5	5 – 10	10 – 30
4- Drainage Density	v. low	low	medium	high	v. high
	0 – 0.8	0.8 – 1	1 – 1.3	1.3 – 1.5	1.5 – 2
5- TWI	v. low	low	medium	high	v. high
	-1.5 – 2	2 – 4	4 – 6	6 – 10	10 – 20
6- Surface Roughness	v. soft	soft	medium	rough	v. rough
7- LST (C)	v. high	high	medium	low	v. low
	52 - 57	50 - 52	48 - 50	46 - 48	40 - 46
8- Acc. Precipitation	v. low	low	medium	high	v. high
	7 - 10	10 - 12	12 - 16	16 - 20	20 - 30
9- LULC	basement/Urban	sed. Rocks	old alluvial deposits	Recent Wadi deposits	vegetation
10- Lineament Density	v. low	low	medium	high	v. high
	0 - 80	80 - 150	150 - 230	230 - 300	300 - 380

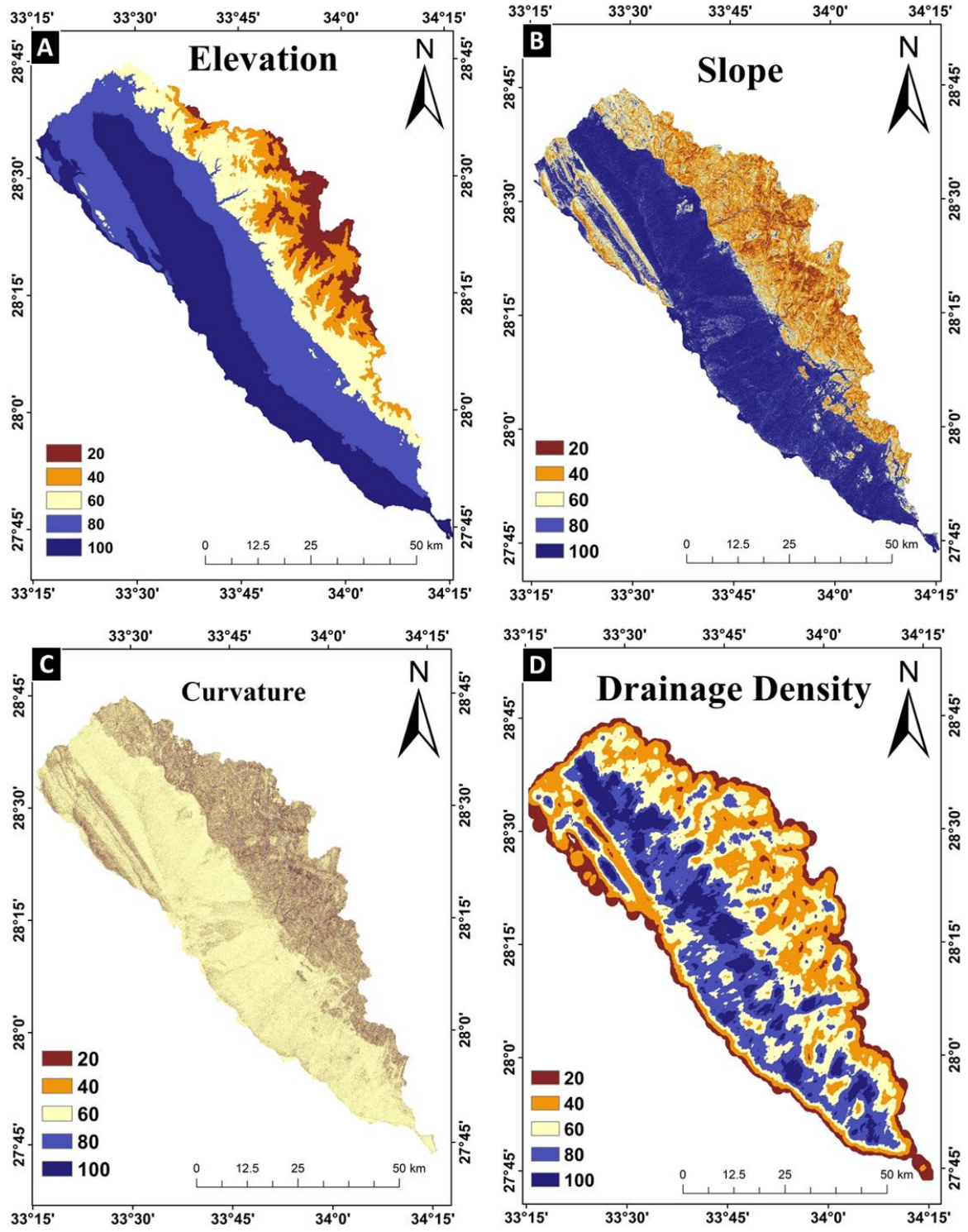

Fig. 6: (A) Elevation weight, (B) Slope weight, (C) Curvature weight, (D) Drainage Density weight.

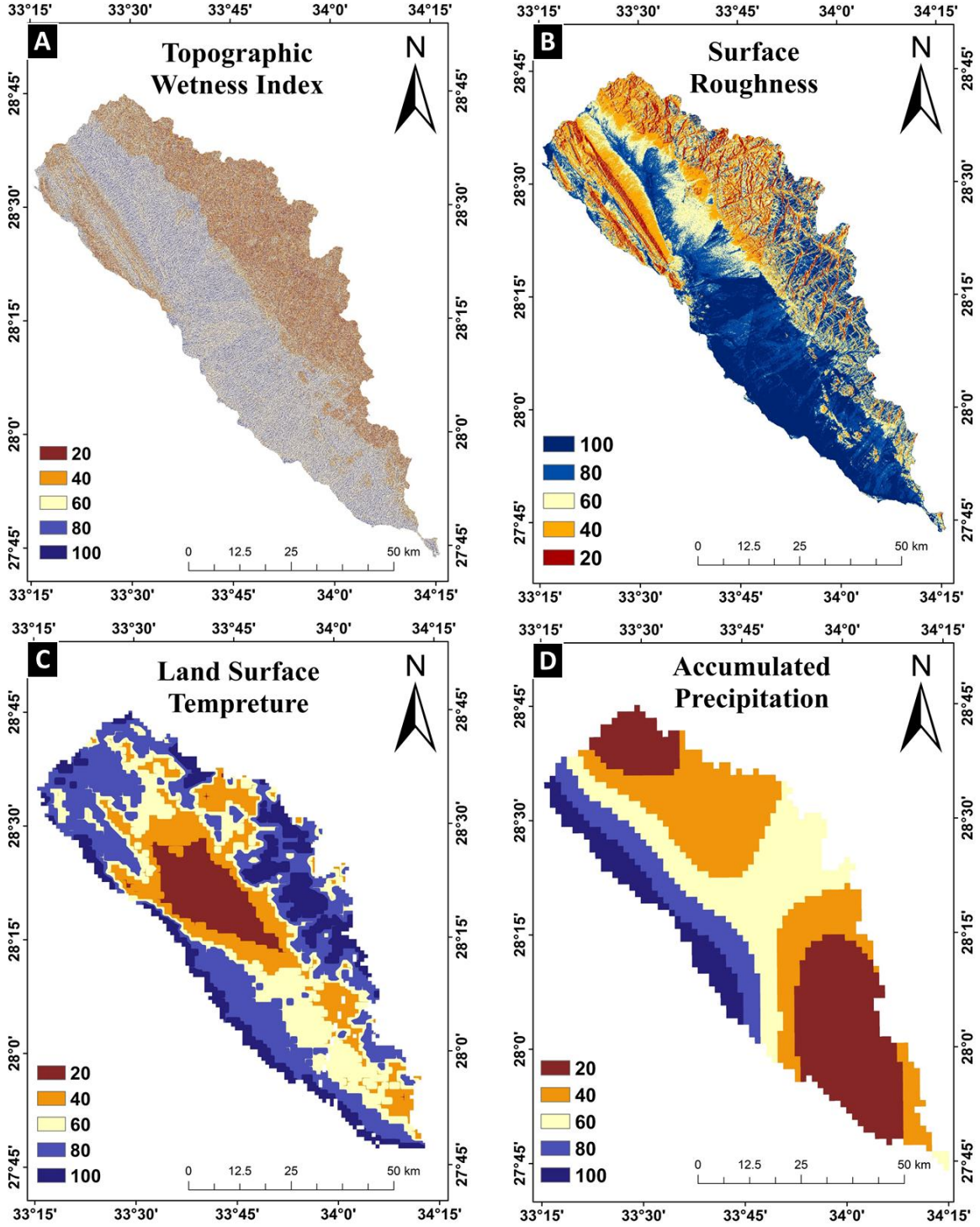

Fig. 7: (A)Topographic Wetness Index weight, (B) Surface roughness weight, (C) LST weight, (D) Accumulated Precipitation weight.

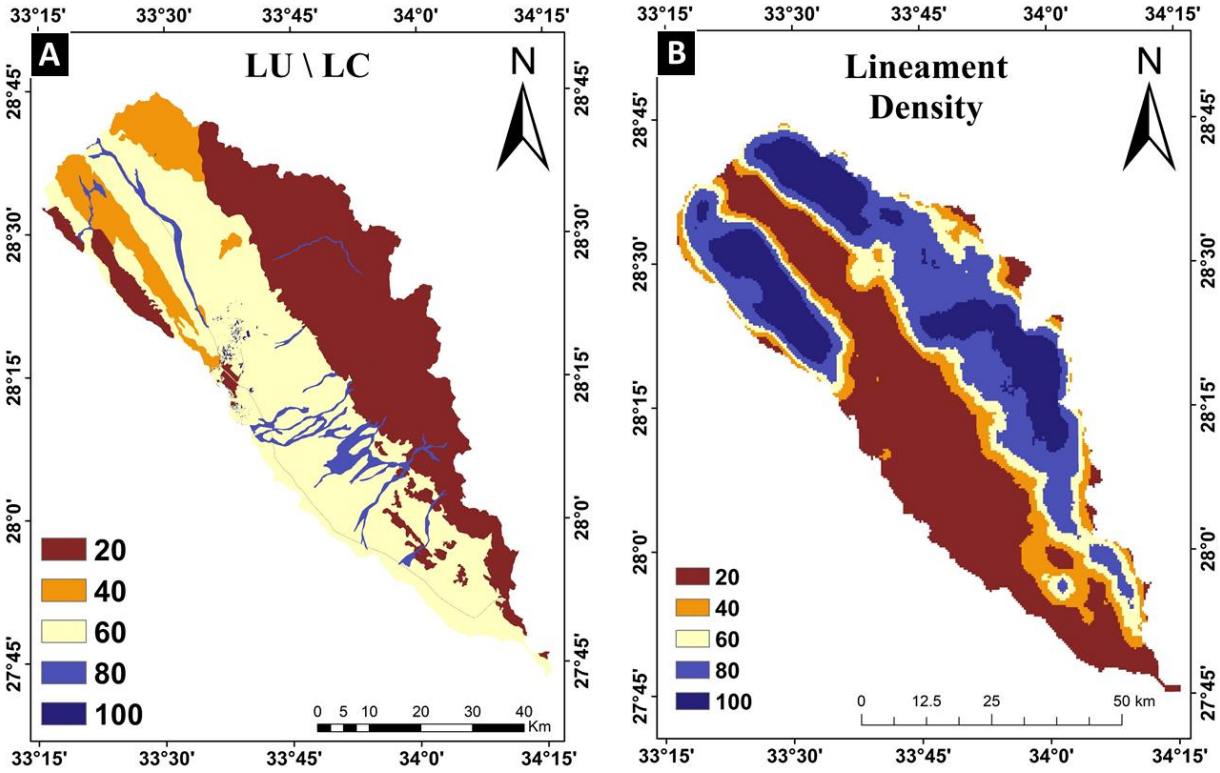

Fig. 8: (A) LU\LC weight, (B) Lineament Density weigh.

4. RESULTS AND DISCUSSION

The resulted GWP map, based on the SAW overlay modeling, was classified into 5 main zones according to their potential for groundwater occurrence: very high (707 - 881), high (637 - 707), medium (566 - 637), low (490 - 566) and very low (158 - 490) (Fig. 9).

The interpretation of the GWP map reveals that most of the very high (VH) zone was defined along Wadi El-Awaj, which drains parallel to the coast line. It also appears along the northern part of Wadi Araba, as well as at the outlet of the other wadies south of El-Tour City; such as W. Isla, W. Moraikh, W. Sid, and W. El-Mahash. In other words, the very high GWP zone is extended continuously from the delta of Wadi Al-Awaj near El-Tour City to the outlet of Wadi Mahash. The extension of this zone along the coastal line is reasonable and can be attributed to the massive runoff that originates from the basement highlands and flows toward the Gulf of Suez coast, where the flow velocity slows down due to the gentle slope and provides optimum conditions for infiltration process.

On the other hand, the high (H) GWP zone is distributed along the rest of the plain between the mountains region and the VH GWP zone. It locates at regions with high lineaments density and surface roughness. The Moderate (M) zone occupies a relatively less portion of the plain and it is mostly located at the mountain foothills and along the northwestern part of the study area near Gebel Qabliat. The low and very low (L and VL) zones are predominately at the eastern basement mountains due to the steep slope and low infiltration conditions. These outcomes conclude that the VH and H GWP was generally associated with low terrain, high surface ruggedness, dense drainage and lineament, relatively close to thermal anomalies, and fluvial wadi deposits or sandy areas.

4.1. Field Validation

The field work of the present study was carried out on April 2018 to validate the remote sensing data results and the accuracy of the produced GWP map, (Fig. 9). The field investigations included, soil infiltration rate,

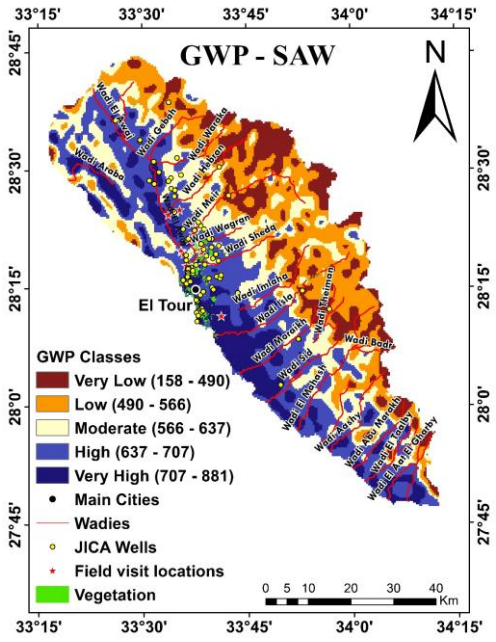

Fig 9: Groundwater Potential map with locations of field verification sites.

collecting water well samples, mapping farms and other vegetation patterns in the study area (Fig. 10). The soil infiltration rate was performed in all land cover classes, which generated based on image classification of the optical sensor.

A primitive 6-inch diameter cylinder infiltrometer was used to measure the infiltration rate for a 500-milliliter water per test, then the time of percolation was recorded. This simple test was applied several times in each landcover class. The results of the soil infiltration rate test were utilized to validate the landcover classes and assign the semi-quantitative weight index for each class.

The field work also includes a projection of all water wells and farm locations on the final GWP map to validate the model assumption for the 5 different GWP zones (Fig. 9). The results show that 35% of the water wells locate in the very high GWP zone, 46% in the high, 15% in the moderate, 2% in the low and 2% in the very low. The majority of these wells were drilled based on geophysical (mainly geoelectric resistivity) investigations and producing good water quality for agricultural purposes. Therefore, the overall accuracy of the produced GWP is roughly estimated at about 81% based on the distribution of the water wells in the study area. However, further geophysical studies at the delineated VH and H GWP zones are recommended in the study area.

Fig. 10: Field validation photos, (A) soil infiltration test at site no. 12, (B) cultivated lands in site no. 8, (C) new water well in site no 3, (D) collecting water sample from site no. 7.

5. CONCLUSION

This study integrates remote sensing data and geospatial techniques for mapping groundwater potential in one of the most promising locations for development in the Sinai Peninsula, which is El-Qaa Plain. The importance of utilizing remote sensing data instead of conventional land-based techniques came to produce continuous surface maps at higher resolutions and consistent scales than previously published maps, as well as to overcome the scarce of surface flow data. Therefore, the main objective of this work is identifying physiographic variables that affecting groundwater recharge and storage for detecting renewable groundwater accumulation.

A wide range of remote sensing data including optical, radar and thermal sensors were used to construct several geospatial thematic layers (variables). These variables include elevation, slope, curvature, drainage density, topographic wetness index, surface roughness, frequency of thermal anomaly, accumulated precipitation, Land Use/Land Cover (LULC) and lineament density. All variables were arranged and weighted based on their contributions in groundwater recharge through infiltration and percolation processes. The Simple Additive Weight (SAW) method was adopted for computing the variables weights and producing the GWP map.

The produced GWP map indicates that most of the very high zone locates along Wadi El-Awaj, the northern part of Wadi Araba, and near the outlets of several wadies south of El-Tour City. The high GWP zone is distributed along the plain and relatively has larger extent than VH zone, especially near the mountains region, where the density of the lineaments and surface roughness increase. By contrast, the low and very low zones are associated with the roughed eastern basement mountains.

A fieldwork was conducted along the study area to validate the remote sensing data results and the accuracy of the produced GWP map through soil infiltration rate, collecting water well samples, mapping farms and other vegetation patterns in El-Qaa Plain. The field work shows that 81% of the water wells locate in the very high and high GWP zones, while 15% in the Moderate, and only 4% in the low and the very low zones. Therefore, the overall accuracy of the produced GWP was roughly estimated at about 81%, but for crucial field validation to the result, further geophysical investigations should be carried out at the defined very high and high GWP zones in the study area. In conclusion, the present study provides a geospatial-based tool to define zones with high groundwater probability for downscaling the exploration efforts via conventional land-based methods and could be applied elsewhere in arid regions.

REFERENCES

Abrams, W., Ghoneim, E., Shew, R., LaMaskin, T., Al-Bloushi, K., Hussein, S., El-Baz, F. (2018). Delineation of groundwater potential (GWP) in the northern United Arab Emirates and Oman using geospatial technologies in conjunction with Simple Additive Weight (SAW), Analytical Hierarchy Process (AHP), and Probabilistic Frequency Ratio (PFR) techniques. *Journal of Arid Environments*, *157*, 77–96. https://doi.org/10.1016/j.jaridenv.2018.05.005

AbuBakr, M. (2014). *Hydrological Modeling by Remote Sensing, GIS and Subsurface Geological Data Integration For Groundwater Exploration and Flash Flood Estimation in Northern Sinai*. Al-Azhar University and Boston Univesity.

AbuBakr, M., Ghoneim, E., El-Baz, F., Zeneldin, M., & Zeid, S. (2013). Use of radar data to unveil the paleolakes and the ancestral course of Wadi El-Arish, Sinai Peninsula, Egypt. *Geomorphology*, *194*, 34–45. https://doi.org/10.1016/j.geomorph.2013.04.005

Adiat, K. A. N., Nawawi, M. N. M., & Abdullah, K. (2012). Assessing the accuracy of GIS-based elementary multi criteria decision analysis as a spatial prediction tool – A case of predicting potential zones of sustainable groundwater resources. *Journal of Hydrology*, *440–441*, 75–89. https://doi.org/10.1016/J.JHYDROL.2012.03.028

Ahmed, A. A. E.-H. (1984). *Geomorphological and hydrogeological studies on Qaa plain, Gulf of Suez, Sinai, Egypt*. Cairo University.

Ahmed, M. E.-S. (2012). Integrated Approach for Hydrogeologic Investigations in Africa :

Inferences from Space- Borne and Land-Based Gravity , Aeromagnetic , GIS , and Remote Sensing Data.

Al-Ruzouq, R., Shanableh, A., & Merabtene, T. (2015). Geomatics for Mapping of Groundwater Potential Zones in Northern Part of the United Arab Emiratis - Sharjah City. *ISPRS - International Archives of the Photogrammetry, Remote Sensing and Spatial Information Sciences*, *XL-7/W3*, 581–586. https://doi.org/10.5194/isprsarchives-XL-7-W3-581-2015

Amer, R., Sultan, M., Ripperdan, R., Ghulam, A., & Kusky, T. (2013). An integrated approach for groundwater potential zoning in shallow fracture zone aquifers. *International Journal of Remote Sensing*, *34*(19), 6539–6561. https://doi.org/10.1080/01431161.2013.804221

Azab, A. A., & El-Khadragy, A. A. (2013). 2.5-D Gravity/Magnetic Model Studies in Sahl El Qaa Area, Southwestern Sinai, Egypt. *Pure and Applied Geophysics*, *170*(12), 2207–2229. https://doi.org/10.1007/s00024-013-0650-5

Bank, T. W. (2010). *Overview: Water Sector Brief*. Retrieved from http://siteresources.worldbank.org/%0AINTMNAREGTOPWATRES/Resources/Water_Sector_Brief Fall2010.pdf

Beven, K. J., & Kirkby, M. J. (1979). A physically based, variable contributing area model of basin hydrology. *Hydrological Sciences Bulletin*. https://doi.org/10.1080/02626667909491834

Dames, & Moore. (1981). Agricultural and water investigation of the Sinai. Desert Institute, Mataria, Cairo, A.R.E.

Egyptian Mineral Resources General Authority, E. (1994). *Geological map of Sinai, sheet no 1, scale 1:250 000*. Cairo.

Elbeih, S. F. (2014). An overview of integrated remote sensing and GIS for groundwater mapping in Egypt. *Ain Shams Engineering Journal*, *6*(1), 1–15. https://doi.org/10.1016/j.asej.2014.08.008

Gaber, A., Koch, M., Griesh, M. H., & Sato, M. (2011). SAR remote sensing of buried faults: Implications for groundwater exploration in the western desert of Egypt. *Sensing and Imaging*, *12*(3–4), 133–151. https://doi.org/10.1007/s11220-011-0066-1

Gemail, K. M. S. (1996). *Shallow Geophysical Exploration for Ground Water around Wadi Isla, Southern Part of EL‐Qaa Plain, Southwestern Sinai, Egypt*. Zagazig University.

Ghoneim, E. (2008). Optimum groundwater locations in the northern United Arab Emirates. *International Journal of Remote Sensing*, *29*(20), 5879–5906. https:// doi.org/10.1080/01431160801932517

Ghoneim, E., & El-Baz, F. (2007). The application of radar topographic data to mapping of a mega-paleodrainage in the Eastern Sahara. *Journal of Arid Environments*. https://doi.org/10.1016/j.jaridenv.2006.11.018

Helba, A. A.-A. (1987). *Geology of Gebel Safariat area, southwest Sinai, Egypt*. Cairo University.

Japan International Cooperation Agency (JICA). (1999). South Sinai groundwater resources study in the Arab Republic of Egypt.

Jenks, G. F. (1967). The Data Model Concept in Statistical Mapping. *International Yearbook of Cartography*. https://doi.org/citeulike-article-id:8241517

Jenson, S. K., Dominque, J. O., & Domingue, J. O. (1988). Extracting Topographic Structure from Digital Elevation Data for Geographic Information System Analysis. *Engineering*, *54*(11), 1593–1600. https://doi.org/0099-1112/88/5411-1593$02.25/0

Khalil, S., & Hendy, E.-A. (1984). Geophysical exploration of buried vallies in El-Qaa Plain, S. W. Sinai, Egypt. In *3rd Annual Meeting of Geophysical Society of Egypt* (pp. 42–54). Cairo.

Laben, C. A., & Brower, B. V. (2000). United States Patent (19) Fig-1, (19). https://doi.org/10.1016/j.(73)

Lee, J. Sen, & Pottier, E. (2017). *Polarimetric radar imaging: From basics to applications*. *Polarimetric Radar Imaging: From Basics to Applications*. https://doi.org/ 10.1201/9781420054989

Lillesand, T. M., & Kiefer, R. W. (1987). *Remote Sensing and Image Interpretation* (2nd ed.). Wiley, New York.

Mallick, J., Singh, C. K., Al-Wadi, H., Ahmed, M., Rahman, A., Shashtri, S., & Mukherjee, S. (2015). Geospatial and geostatistical approach for groundwater potential zone delineation. *Hydrological Processes*, *29*(3), 395–418. https://doi.org/10.1002/hyp.10153

Manap, M. A., Sulaiman, W. N. A., Ramli, M. F.,

Pradhan, B., & Surip, N. (2013). A knowledge-driven GIS modeling technique for groundwater potential mapping at the Upper Langat Basin, Malaysia. *Arabian Journal of Geosciences*, *6*(5), 1621–1637. https://doi.org/10.1007/s12517-011-0469-2

Masoud, A. A. (2009). Runoff modeling of the wadi systems for estimating flash flood and groundwater recharge potential in Southern Sinai, Egypt. *Arabian Journal of Geosciences*, *4*(5), 785–801. https://doi.org/10.1007/s12517-009-0090-9

Mccauley, J. F., Schaber, G. G., Breed, C. S., Grolier, M. J., Haynes, C. V., Issawi, B., … Blom, R. (1982). Subsurface valleys and geoarcheology of the Eastern Sahara revealed by shuttle radar. *Science*. https://doi.org/ 10.1126/science.218.4576.1004

Naghibi, S. A., Pourghasemi, H. R., Pourtaghi, Z. S., & Rezaei, A. (2015). Groundwater qanat potential mapping using frequency ratio and Shannon's entropy models in the Moghan watershed, Iran. *Earth Science Informatics*, *8*(1), 171–186. https://doi.org/ 10.1007/s12145-014-0145-7

Salem. (1990). *report on southern Sinai fild trip for risk evaluation of flash floods, institute for water resources development*. Sinai.

Sherief, Y. S. Y. (2008). *Flash floods and their effects on the development in El-Qaá plain area in South Sinai, Egypt, a study in applied geomorphology using GIS and remote sensing*. Johannes Gutenberg University Mainz.

Smith, M. J., & Wise, S. M. (2007). Problems of bias in mapping linear landforms from satellite imagery. *International Journal of Applied Earth Observation and Geoinformation*. https://doi.org/ 10.1016/ j.jag.2006.07.002

Sørensen, R., Zinko, U., & Seibert, J. (2006). On the calculation of the topographic wetness index: Evaluation of different methods based on field observations. *Hydrology and Earth System Sciences*, *10*(1), 101–112. https://doi. org/10.5194/hess-10-101-2006

Sultan, M., Metwally, S., Milewski, A., Becker, D., Ahmed, M., Sauck, W., Welton, B. (2011). Modern recharge to fossil aquifers: Geochemical, geophysical, and modeling constraints. *Journal of Hydrology*, *403*(1–2), 14–24. https://doi.org/10.1016/j. jhydrol. 2011.03.036

Wan, Z., Hook, S., & Hulley, G. (2015). MYD11A1 MODIS/Aqua Land Surface Temperature/ Emissivity Daily L3 Global 1km SIN Grid V006 [Data set]. NASA EOSDIS LP DAAC. https://doi.org/10.5067/MODIS/MYD11A1.0 06

Weier, J., & Herring, D. (2018). Measuring Vegetation (NDVI & EVI) : Feature Articles. https://doi.org/10.1111/j.1365-246X.2011.05323.x

دمج التقنيات الجيومكانية لتحديد الأماكن المحتملة لتواجد المياه الجوفية بمنطقة سهل القاع، جنوب غرب سيناء، مصر

محمود يسري زين الدين[١]، مصطفى أبو بكر[١]، رمضان غريب هارون[٢]، ممدوح محمد علي[٢]

قسم الجيولوجيا، جامعة الأزهر، مدينة نصر، القاهرة، مصر١
الهيئة المصرية العامة للثروة العدنية، القاهرة، مصر٢

تمثل المياه الجوفية المصدر الأساسي للمياه العذبة في معظم المناطق القاحلة مثل شبه جزيرة سيناء. يتطلب استكشاف موارد المياه الجوفية في الأراضي الجافة إجراء مسح لمناطق شاسعة باستخدام تقنيات أرضية تقليدية. تقوم هذه الدراسة بالتنقيب عن المياه الجوفية في الجزء الجنوبي الغربي من شبه جزيرة سيناء من خلال تحديد الاماكن المحتملة لتواجد المياه الجوفية باستخدام تقنيات الاستشعار عن بعد والتقنيات الجيومكانية المتقدمة إلى جانب التحقق الميداني، كأداة مكملة للطرق التقليدية التي تعتمد على المسح الأرضي بشكل أساسي. الهدف الرئيسي من الدراسة هو تحديد ودراسة تأثير المتغيرات الطبوغرافية على تواجد وتراكم المياه الجوفية. لذلك، تم استخدام عدد من البيانات المستخلصة من العديد من الأقمار الصناعية ASTER, Landsat-8, MODIS, SRTM, TRMM و RADARSAT-1 لبناء عدة طبقات جيوغرافيه والتي تم ترتيبها وترجيحها على أساس مساهماتها في تغذية المياه الجوفية من خلال عمليات الترشيح. وتشمل هذه الطبقات الارتفاعات، الميول، درجة الانحناء، كثافة شبكات التصريف، مؤشر الرطوبة، خشونة السطح، تغيرات درجة حرارة السطح، كمية الامطار، استخدامات الأراضي وكثافة التراكيب السطحية. تم استخدام طريقة الوزن الإضافي البسيط (SAW) لحساب أوزان المتغيرات وإنتاج خريطة توضح احتماليات تواجد المياه الجوفية تحتوي على ٥ فئات، تتراوح من المناطق ذات الاحتماليات العالية جداً إلى المنخفضة جداً. تتواجد الأماكن ذات الاحتمالية العالية على طول وادي الأعوج والاجزاء الشمالية من وادي عربة وقرب مخارج الاودية جنوب مدينة الطور. ولوحظ ان الأماكن التي لها احتماله عالية لتواجد وتراكم المياه الجوفية تكون مصاحبة للاماكن ذات الارتفاعات المنخفضة وذات الاسطح الخشنة والتي بها كثافة عالية من الاودية والتراكيب السطحية بالإضافة الي انها أيضا تكون مصاحبة للرواسب الوديانية ذات درجات الحرارة المنخفضة. تم التحقق من صحة النتائج من خلال الزيارات الميدانية بما في ذلك قياس معدلات الترشيح للتربة، وبيانات آبار المياه والاماكن التي بها زراعات داخل منطقة الدراسة. استناداً إلى النتائج النهائية، يمكن أن توفر بيانات الاستشعار عن بعد جنباً إلى جنب مع التقنيات الجيومكانية أداة قوية للتنقيب عن المياه الجوفية في الأراضي القاحلة بالتكامل مع الطرق الجيوفيزيائية، وبالتالي يمكن تطبيقها في المناطق ذات الظروف المماثلة، مثل دول الشرق الأوسط.